Effects of Bovine Serum Albumin and Hyaluronic Acid on the Electrochemical Response of a CoCrMo Alloy to Cathodic and Anodic Excursions

S. Radice[1] · S. Liu[1,2] · R. Pourzal[1] · M. P. Laurent[1] · M. A. Wimmer[1]

Abstract

The problem of wear and corrosion of CoCrMo-implant surfaces in the human body following total joint replacement has been commonly investigated with tribocorrosion tests, using different lubricants meant to simulate the pseudo-synovial fluid. While results considering the synovial fluid components separately have highlighted their individual influence on the tribological performance of CoCrMo-alloy, an understanding about the influence of the synovial fluid components under the electrochemical point of view is missing. This work aims to investigate the effect of bovine serum albumin (BSA) and hyaluronic acid (HA) on electrochemical potential variations of CoCrMo alloys tested in a model synovial fluid. To simulate the environment inside the synovial capsule, the tests were performed inside a CO_2 incubator at 37 °C. Open circuit potential, electrochemical impedance spectroscopy, cathodic and anodic potentiodynamic measurements were performed with different electrolytes, prepared with cell culture medium (RMPI-1640), BSA and HA. The final CoCrMo-surface was analyzed by SEM/EDS and infrared spectroscopy. The influence of HA on the corrosion of the CoCrMo-alloy depended on the presence of BSA proteins adsorbed on the CoCrMo-surface: EIS and anodic polarization results showed a corrosive action of HA in the absence of adsorbed proteins. In the presence of both BSA and HA, organometallic precipitates were found on the CoCrMo surface following reverse anodic polarization, which remind of corrosion products found in vivo. These results indicate that HA affects the interaction of CoCrMo implant alloys with protein-containing model synovial fluids, and suggest that HA needs to be considered in tribocorrosion studies for more clinically relevant outcomes.

Keywords Cobalt–chromium alloy · Corrosion · Synovial fluid · Hyaluronic acid · Albumin

1 Introduction

Total joint replacement is a common and well-established orthopedic surgical operation worldwide. The most used metallic implant materials are CoCrMo- and TiAlV- alloys. CoCrMo alloy has outstanding mechanical properties and corrosion resistance. Still, the surface of the CoCrMo implant may undergo significant alterations over its lifetime. Processes of surface alterations, such as tribocorrosion [1–8], can have negative effects on implant performance.

They may also have positive effects, like the formation of a protective, lubricous film, increasing the alloy service life [9–15].

The question of surface alteration of CoCrMo-implants in the human body following total joint replacement has been widely investigated, mostly from the tribological point of view [16–20]. Several studies have integrated electrochemical measurements into the tribological system to describe the tribocorrosion behavior of CoCrMo-implants in different simulated body fluids [3, 21]. For both tribological and tribocorrosion studies, phosphate buffer saline solution and bovine serum diluted up to 25% in saline solutions have been commonly chosen as model synovial fluids [3, 21]. The combination of serum and saline solution is meant to reproduce both salt and protein content of the synovial fluid. More complex model fluids that include hyaluronic acid (HA) and phospholipids in addition to proteins and physiological salinity have been

✉ S. Radice
  simona_radice@rush.edu

1   Department of Orthopedic Surgery, Rush University Medical
    Center, Chicago, IL 60612, USA

2   Department of Bioengineering, University of Illinois
    at Chicago, Chicago, IL 60607, USA

recently proposed and tested for friction and wear [19, 20, 22, 23]. Results from tribological testing, considering the synovial fluid components separately, show that proteins and HA enhance lubrication through the formation of a boundary organic lubricant layer and an increase of the viscosity of the fluid [19, 20].

Some studies have focused exclusively on the electro-chemical behavior of CoCrMo-surfaces in model synovial fluids [24–29]. In particular, the role of albumin as the most abundant protein in the synovial fluid has been inves-tigated, with conclusions regarding the interaction of albu-min with CoCrMo-surfaces at different electrochemical potentials, both in the cathodic and anodic domain. Under cathodic conditions and physiological concentrations (~ 30 g/L), BSA was found to form thick adsorption films and to modify the passive film composition of CoCrMo alloys, inhibiting oxygen reduction and promoting water reduction [30]. In terms of electrochemical behavior, BSA tested with lower concentrations (0.005–0.5 g/L) was found to act as a cathodic inhibitor and as an anodic cata-lyzer [28, 29]. Less information is available in the litera-ture about the electrochemical behavior of CoCrMo-alloys in HA containing electrolytes. In [25], the presence of HA in simulated Hank's physiological solution in immersion tests of CoCrMo-alloy was shown to stimulate the forma-tion of a calcium phosphate layer and up to 24 h were needed for the open circuit potential (OCP) to stabilize; the length of immersion time at the OCP (1 h vs. 10 h) had an effect on the shape of the anodic polarization curves; in the presence of HA these curves were shifted towards an anodic (more noble) potential. The electrolytes used did not contain proteins, and information about possible inter-actions between HA and proteins and their influence on the electrochemical behavior of CoCrMo-alloys is missing. In preparation for the present work, no publications about the electrochemical role of HA in combination with BSA were found.

The aim of this study was to investigate the effects of HA, BSA and a combination of HA and BSA in model synovial fluids, on the electrochemical response of a medical grade wrought low-carbon CoCrMo alloy to cathodic and anodic excursions. Separate cathodic and anodic polarization meas-urements starting from the OCP (instead of a cathodic-to-anodic polarization) have been recently used by different authors in the field [25, 30]. This approach allows investigat-ing possible in vivo electrochemical reactions. In fact, local anodic and cathodic potential excursions are likely to occur at the surface of a metallic implant upon local removal of passive oxide layer by fretting or wear [30], which is also plausibly related to local alteration of the fluid concentration and properties (for example HA degradation due to inflam-mation). It was hypothesized that the HA and BSA would interact in their effect on the alloy.

2 Materials and Methods

2.1 CoCrMo-Samples

Wrought low-carbon CoCrMo disks, 12 mm in diameter and 7 mm in height, were cut from medical grade bar stock (Aubert & Duval Corporation, Bolingbrook, IL, USA). The chemical composition of this alloy follows ASTM F1537 and ISO 5832-12 standards and is given by the manufacturer as follows (values in wt%): Carbon: < 0.14; Chromium: 28.00; Molybdenum: 6.00; Nickel: < 1.00; Cobalt: Base; with the addition of nitrogen. The disks' surfaces were ground and mirror-polished on a semi-auto-matic Struers MD Gecko machine from SiC foil # 320 up to 1 µm diamond paste. Final surface roughness values as measured on a Scanning White Light Interferometer (Zygo NewView 6300, Zygo Corp., Middlefield, CT, USA) were in the order of $R_a = 10$ nm, consistently with the surface finish of the commercial hip-replacement components [26].

2.2 Electrolytes

Cell culture medium (RPMI-1640, Catalog No. 11875093, ThermoFisher Scientific) was used as base solution. Its complete formulation is available online at the company's website. The concentrations of the main amino acids and vitamins are given in [31]. RPMI-1640 is composed of different amino acids, vitamins, inorganic salts, D-Glucose, reduced Glutathione and Phenol Red (the latter for moni-toring of the pH). Phenol Red confers the medium to a red/pinkish color at pH 7.3–8.0, an orange/reddish color at pH 6.7–7.2 and a yellowish color at pH 6.0–6.6.

Four different electrolytes were tested. The first consisted of cell culture medium RPMI-1640 only and was the control group. The second electrolyte was RPMI-1640-containing 30 mg/mL of bovine serum albumin (BSA) powder (Catalog No. B14, ThermoFischer Scientific). The third was RPMI-1640 containing 3 mg/mL of Hyaluronic Acid (HA) sodium salt from streptococcus equi (Catalog No. 53747, Sigma-Aldrich). Finally, the fourth was given by a combination of the previous two, with 30 mg/mL BSA and 3 mg/mL HA. The concentrations of proteins and HA were chosen to rep-resent the synovial fluid in diseased joints [19].

The BSA was added 30 min before the test for any BSA-containing electrolyte. Dissolving of BSA was facilitated by a Vortex machine. HA was added the evening before the day of the test and gently mixed overnight by a magnetic stirrer at room temperature. The preparation of the elec-trolytes was carried out under a laminar flow hood with particular care for keeping the sterility of the solutions.

2.3 Electrochemical Setup

A three-electrode electrochemical cell configuration connected to a potentiostat (Series G750, Gamry Instruments) was used for the tests (Fig. 1).

The custom made cell was a cylindrical chamber made of polyether ether ketone (PEEK) with 20 mL volume capacity. The working electrode consisted of a CoCrMo disk sample. The disk was fitted in the middle of the chamber, exposing its polished surface only. An O-ring sealed the disks laterally at the top edge, so that a disk surface area of 1.131 cm^2 had electrolyte exposure. A drill hole (diam. 4 mm) at the bottom of the PEEK chamber allowed for electric contact between the metal sample and the working electrode plug of the potentiostat. A Silver/Silver Chloride Skinny Reference Electrode (Gamry Instruments) in saturated KCl solution was obliquely held at approximately 2 mm from the CoCrMo-disk surface. A 0.5 mm diam. platinum (Pt) wire (annealed, 99.95% metals basis, Fischer Scientifics) was used as the counter electrode. The Pt wire was anchored circumferentially along the wall. The theoretical surface ratio between the counter electrode and the working electrode was 2.8.

2.4 Testing Protocol and Characterization Tools

The tests were performed inside a water-jacketed CO$_2$ incubator (Model 2460, Shel Lab, OR, USA). The temperature was set to 37 °C and the CO$_2$ level to 5.0%. To equilibrate, the electrolyte was placed inside the incubator 30 min before the test. The bulk electrolytes' pH stayed in the range 7.0–7.5, as verified visually (red/pinkish

Fig. 1 Illustration of the three-electrode electrochemical chamber. *WE* (Working Electrode): CoCrMo; *CE* disk (Counter Electrode): Platinum wire; *RE* (Reference Electrode): Silver/Silver Chloride Ag/AgCl electrode

coloration of the fluid) and using pH papers. The pH value was held constant utilizing the buffer effect of the sodium bicarbonate in the cell culture medium RPMI-1640 working in concert with the controlled CO$_2$ environment.

The CoCrMo-disks were ultrasonically cleaned in isopropanol for 10 min, rinsed under tap bidistilled water (Elix Millipore 15), ultrasonically cleaned in bidistilled water for 10 min and immediately placed inside the test chamber. The test chamber was generously rinsed under tap bidistilled water, dried with N$_2$ gas flow and immediately placed inside the incubator. The reference electrode was rinsed with bidistilled water, sprayed with 70 vol% ethanol solution and rinsed again with bidistilled water before being positioned in the test chamber (already inside the incubator). The cables were connected and the electrolyte was poured into the chamber. The test was started once the temperature and the CO$_2$ level had almost reached the set values ($T > 35.5$ and CO$_2 > 4.7$). The following steps were performed on the Gamry Framework (version 6.25): (1) Open Circuit Potential stabilization for 1–3 h (called here "Initial Open Circuit Potential", OCP$_i$); (2) Potentiostatic Electrochemical Impedance Spectroscopy from 50 kHz to 0.005 Hz with 10 mV (rms) versus E_{OP} (EIS); (3) Cathodic Polarization with forward and reverse scan between OCP and − 0.9 V versus E_{OP}, and scan speed 2 mV/s; (4) Open Circuit Potential stabilization for 1 h (called here "Intermediate Open Circuit Potential", OCP$_m$); (5) Anodic Polarization with forward and reverse scan between OCP and + 1.4 V versus E_{OP}, and scan speed 2 mV/s (called here "Anodic Polarization"). All potentials presented in the results refer to the Ag/AgCl reference electrode, the standard potential of which is 0.197 V versus SHE [32].

The cathodic vertex potential of − 0.9 V versus E_{OP} was chosen to allow for involved reactions up to the water reduction, which starts below − 1 V versus Ag/AgCl [30] (the OCP being around − 0.1 V versus Ag/AgCl in all tested electrolytes). The anodic vertex potential of + 1.4 V versus E_{OP} was chosen to include the potential domain, where Cr^{6+} is generated, which is around + 0.75 V versus SCE [33]. The scan speed value was adopted from previous experiments in our laboratory [13].

Test were run in triplicates. After each test, the CoCrMo-disks were rinsed with bidistillied water and dried with nitrogen gas. In the absence of visible precipitation products, the disks were ultrasonically cleaned in bidistilled water and in isopropanol and dried with a N$_2$ gas flow for further analysis. The final CoCrMo-surfaces were documented and analyzed using SEM/EDS (JEOL JSM-6490LV). Additional measurements were carried out on a FTIR Spectrometer (Cary 600 Series, Agilent Technologies).
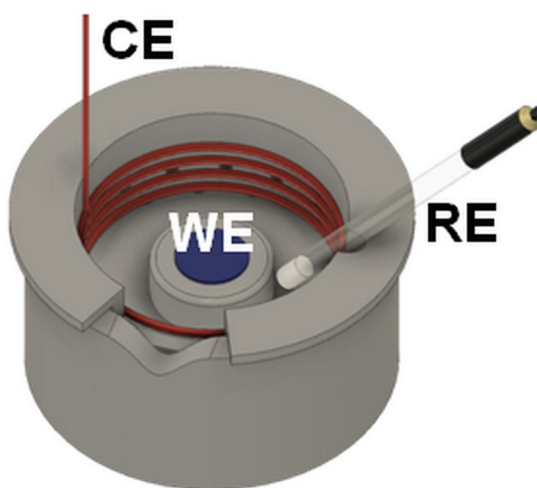
3 Results

3.1 Open Circuit Potential (OCP)

The initial OCP stabilization took 1 h for RPMI and RPMI + BSA, and up to 3 h for RPMI + HA and RPMI + BSA + HA. In Table 1, the slope of OCP, given in mV/min, provides a quantitative indication of the OCP stability. The OCP may be considered stable if OCP fluctuations are smaller than 1 mV/min during a minimum of 1 h [34]. The following general trends were observed (see Table 1): the average OCP_i final value after 1 h was slightly lower in the BSA-containing electrolyte compared to RPMI only; the addition of HA caused an increase in the average OCP_i final values compared to the same electrolyte without HA.

3.2 Electrochemical Impedance Spectroscopy (EIS)

Bode and Nyquist plots from the EIS measurements are given in Fig. 2. On the Bode plot (Fig. 2a), measurements at sufficiently low frequencies correspond to the sum of the resistance of the bulk electrolyte and the polarization resistance. However, the phase did not reach zero at the lowest frequency in these measurements, so that the polarization resistance cannot be directly seen on the Bode plot. Additionally, the number of time constants is not clearly visible from these diagrams. Therefore, equivalent circuit analysis was performed (Table 2). Equivalent circuit models were chosen according to the expected interactions between electrolyte species and the CoCrMo-surface, and to the best fits (lowest Chi-squared values for the fit, and lowest errors for the parameters in the fit): a circuit with an inner resistance and capacitance for the passive oxide film, in parallel with an outer resistance and capacitance of an outside film, was chosen in the case of RPMI, RPMI + HA, and RPMI + HA + BSA [28, 35]; a circuit with an inner resistance and capacitance overlapping with a porous or

Table 1 Initial open circuit potential (OCPi) measured after 1–3 h: average values for the different electrolytes tested (average values ± standard deviation)

Electrolyte	Number of tests	$OCP_i \pm SD$ (V vs. Ag/AgCl)	Max. stabilization time (h)	OCP_i slope (mV/min)
RPMI	$N = 3$	-0.117 ± 0.014	1	≤ 0.3
RPMI + BSA	$N = 3$	-0.155 ± 0.002	1	≤ 0.6
RPMI + HA	$N = 2$	-0.078 ± 0.062	3	≤ 1.1
RPMI + HA + BSA	$N = 2$	-0.126 ± 0.011	3	≤ 0.1

The slope values refer to the last hour for OCPi
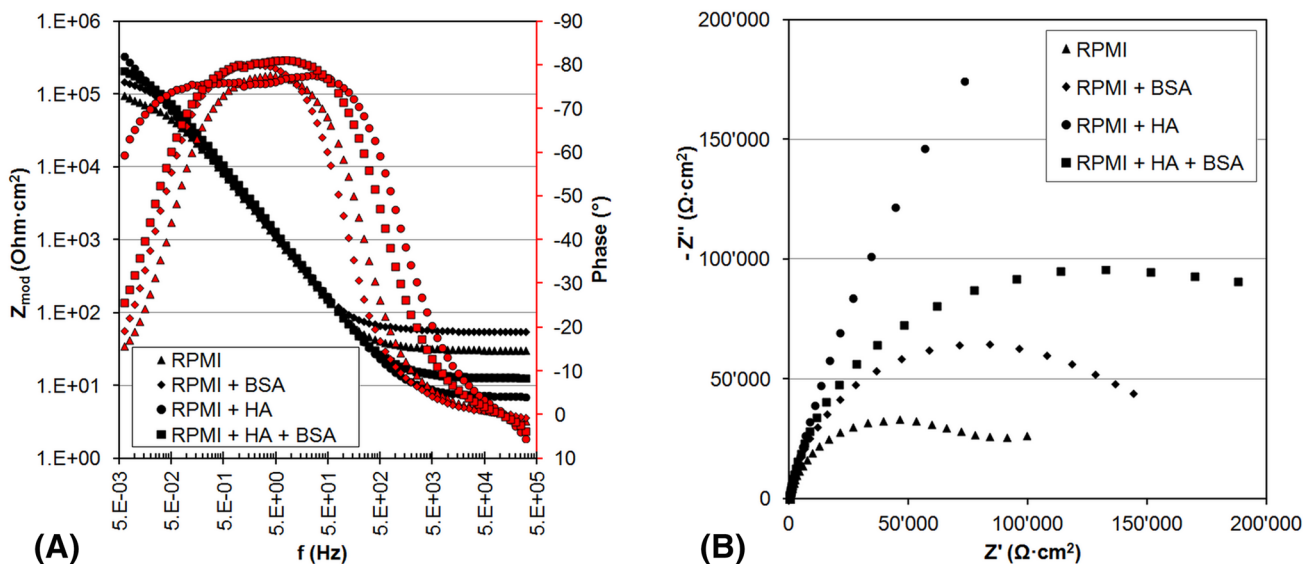
Fig. 2 Bode (**a**) and Nyquist (**b**) plots from one representative EIS measurement for each of the electrolyte groups: RPMI, RPMI + BSA, RPMI + HA, RPMI + HA + BSA

Table 2 Equivalent circuit (EC) parameters fitting the EIS plots of Fig. 2, with illustration of the model EC

Electrolyte/circuit parameter	RPMI	RPMI+BSA	RPMI+HA	RPMI+HA+BSA
EC				
R_s ($\Omega*\text{cm}^2$)	32 ± 0.2	55 ± 0.4	7 ± 0.1	13 ± 0.1
R_{out} (k$\Omega*\text{cm}^2$)	68 ± 12	0.04 ± 0.01	928 ± 71	0.002 ± 0.0005
Q_{out} (μS*s$^\alpha$/cm^2)	103 ± 37	29 ± 2	50 ± 2	50 ± 76
α_{out} (−)	0.8 ± 0.01	0.9 ± 0.02	0.9 ± 0.01	0.9 ± 0.2
R_{in} (k$\Omega*\text{cm}^2$)	32 ± 14	157 ± 3	3 ± 1.6	228 ± 4
Q_{in} (μS*s$^\alpha$/cm^2)	77 ± 20	10 ± 2	287 ± 98	36 ± 0.3
α_{in} (−)	0.9 ± 0.03	1.0 ± 0.02	0.8 ± 0.02	0.9 ± 0.002
Chi squared (−)	1.2 E–03	2.8 E–04	1.2 E–03	9.8 E–04

inhomogeneous outer resistance and capacitance was chosen for RMPI+BSA [27, 36]. A constant phase element (CPE) was used to better represent the non-ideal capacitive behavior of the equivalent circuit capacitances. The equivalent circuits and the calculated parameters are reported in Table 2. By comparing the parameters among the electrolyte groups, it results that: the polarization resistance of the CoCrMo-alloy, closely related to R_{in}, was lowest in RPMI+HA; at the same time, the electrolyte RPMI+HA showed the highest outer resistance R_{out}. Correspondingly, the inner and outer capacitive elements were, respectively, the highest (Q_{in}) and lowest (Q_{out}) in RPMI+HA. The presence of proteins in the HA containing RPMI compensated for the loss of corrosion resistance of the oxide film: R_{in} was highest in RMPI+HA+BSA, with the outer layer showing the lowest R_{out}. These results will be discussed together with the polarization and surface analysis results.

3.3 Cathodic and Anodic Polarization

The plots from the *cathodic polarization* measurements for each group showed good reproducibility, and all plots showed a very similar behavior for the whole cycle. In Fig. 3, the plot for the first test run for each electrolyte is displayed. In the *cathodic forward scan*, the dominant reactions were the reduction of oxygen and water, with hydrogen (gas) evolution. Additionally, a reduction of the original chromium-oxide layer possibly took place. No cathodic inhibition was seen, because the oxygen reduction was limited by the presence of dissolved CO_2 in the electrolyte. The presence of either BSA or HA, or both BSA and HA in combination, did not alter the dominant reduction reactions at the electrode, as
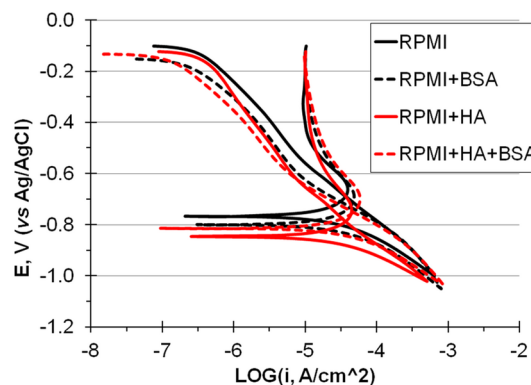
Fig. 3 Representative plots from the cathodic cyclic polarization measurement for each of the electrolyte groups: RPMI, RPMI+BSA, RPMI+HA, RPMI+HA+BSA

no clear differences were seen in the plots from the groups BSA, HA or BSA+HA, compared to RPMI only (Fig. 3). The *reverse cathodic scans* in all plots revealed a transition from dominant cathodic current to dominant anodic current, related to the reduction of passive film in the forward scan. The potential at which this transition occurred is called here cathodic E_{CORR} (corrosion potential). As the potential continued to increase, the anodic current increased up to a shoulder, after which diffusion-limited current behavior was observed up to the end of the cycle (see plateau), reflecting the growth of the passive oxide film. In the presence of BSA and independently from HA, the cathodic E_{CORR} showed a shift to more negative values (Table 3). This finding was in agreement with the OCP_i values. Before starting the anodic polarization, the OCP was let stabilize for 1 h. The OCP_m

Table 3 Cathodic corrosion potential (E_{CORR}) and anodic reverse peak potential (E_{ARP}) average values with standard deviation measured during the cathodic and anodic cyclic polarization scans for all tested electrolytes

Electrolyte	Number of tests	Cathodic $E_{CORR} \pm$ SD (V vs. Ag/AgCl)	$E_{ARP} \pm$ SD (V vs. Ag/AgCl)
RPMI	$N = 3$	-0.777 ± 0.021	0.587 ± 0.008
RPMI + BSA	$N = 3$	-0.803 ± 0.006	0.618 ± 0.052
RPMI + HA	$N = 2$	-0.793 ± 0.049	0.782 ± 0.008
RPMI + HA + BSA	$N = 2$	-0.805 ± 0.015	0.723 ± 0.051

values reached values close to the OCP$_i$ values for all electrolytes. According to the results of statistical t Test analysis (paired two sample for means with $t = 0.05$), OCP$_i$ and OCP$_m$ values within each group were not statistically different ($P > 0.05$), with exception for RPMI ($P = 0.035$). The step of anodic polarization was therefore started at electrochemical conditions, which we considered to be equivalent to the conditions of start of the cathodic polarization.

The plots from the anodic polarization measurements for each group showed good reproducibility, and all plots showed a very similar behavior for the whole cycle. The plot for the first test run for each electrolyte is shown in Fig. 4. In the anodic forward scans, the current behavior in the passive domain did not show a clear plateau for any of the tested electrolytes, as would be expected for a self-passivating alloy. This means, that other oxidizing species present in the electrolyte were reacting in parallel to the oxidation of the CoCrMo-surface. Increasing the potential up to $+1.0$ V in the transpassive domain, the measured current corresponds to oxidation of alloy elements, for example of Cr^{3+} to Cr^{6+}, along with water oxidation and oxygen evolution [37]. The reverse anodic scans showed a negative potential peak setting a transition from dominant anodic to cathodic
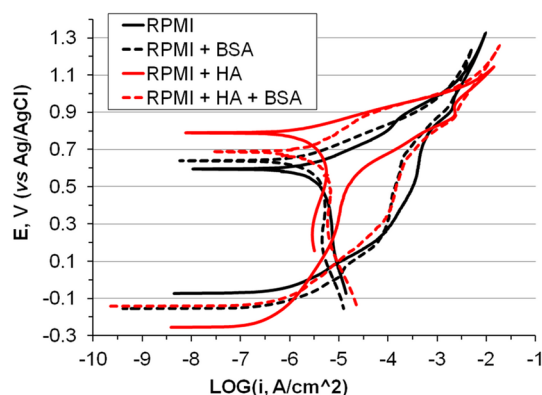
current. The potential, at which this negative peak occurred, is called here "anodic reverse peak potential" (E_{ARP}); it cannot be called "anodic corrosion potential", because a corrosion potential marks a transition from cathodic to anodic current, while this characteristic potential marks a transition from anodic to cathodic current. The following general trends were observed (see Table 3): in the presence of HA and independently from BSA (groups RPMI + HA and RPMI + HA + BSA), the anodic reverse peak potential (E_{ARP}) showed more positive values than in RPMI and RPMI + BSA, indicating the formation of organic films and/or the precipitation of oxidation products covering the surface in these conditions, which block the surface to reverse electrochemical reactions. After this transition, the cathodic current increased up to a diffusion-limited current behavior followed by a slight increase in cathodic current. Moreover, after the tests with HA containing electrolytes, the typical red-pinkish coloration of the medium turned yellowish, but only in a restricted volume above the CoCrMo disk (Fig. 5). This means, that a local pH decrease was apparently more accentuated in the HA containing electrolytes.

3.4 Surface Analysis of the CoCrMo-Disks

After the tests with RPMI, RPMI + BSA and RPMI + HA, films reflecting different colors were seen on the surfaces of the CoCrMo-disks. The colors appeared mostly in concentric patterns due to the geometrical configuration of the three-electrode cell. The optical interference colors ranged from yellow to purple, suggesting a non-perfectly uniform film thickness ranging from 50 to 300 nm [38]. After the
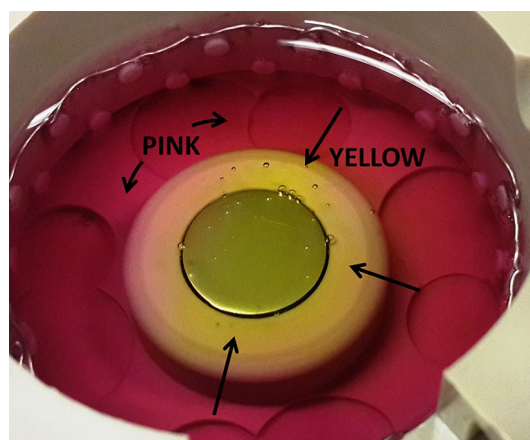

Fig. 4 Representative plots from the anodic cyclic polarization measurement for each of the electrolyte groups: RPMI, RPMI + BSA, RPMI + HA, RPMI + HA + BSA


Fig. 5 Local change of color at the CoCrMo-disk (working electrode) after a test with RPMI + HA: the yellowish coloration indicating a pH decrease can be seen over the metallic surface and partially over the gray PEEK sample holder, in contrast with the pinkish coloration of the electrolyte in the rest of the chamber. The different colorations arise from phenol red, a pH indicator, in the electrolyte (Color figure online)

tests with RPMI + HA + BSA, the disks were found to be covered by a viscous, yellowish gel that remained on the surface even after rinsing with distilled water (Fig. 6a). When air-dried, the gel turned into a green, brittle coating, which had the tendency to delaminate from the metallic surface (Fig. 6b). Isolated flakes of this coating were chosen for additional analyses. Below the green coating, an opaque white film became visible, which adhered firmly to the surface (Fig. 6c).

Observation under the SEM (Fig. 7) in combination with EDS analysis (Table 4) allowed to quantify the chemical composition of the films. Nominal values for the CoCrMo-surface [39] are reported in Table 4 for comparison.
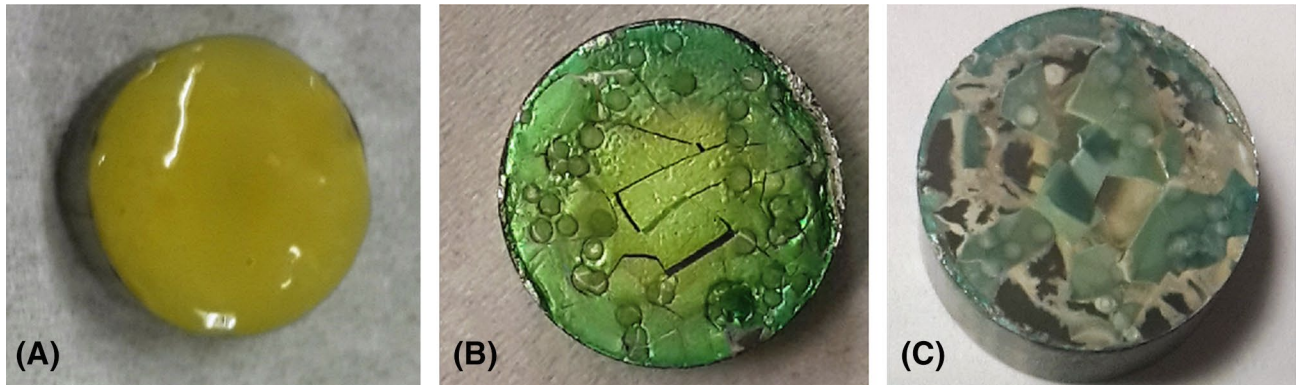

Fig. 6 Digital images of the coating deposited on the metallic surface after the tests with RPMI + HA + BSA: **a** right after the test; **b** dried in air; **c** delaminated coating and partial film coverage of the metal surface
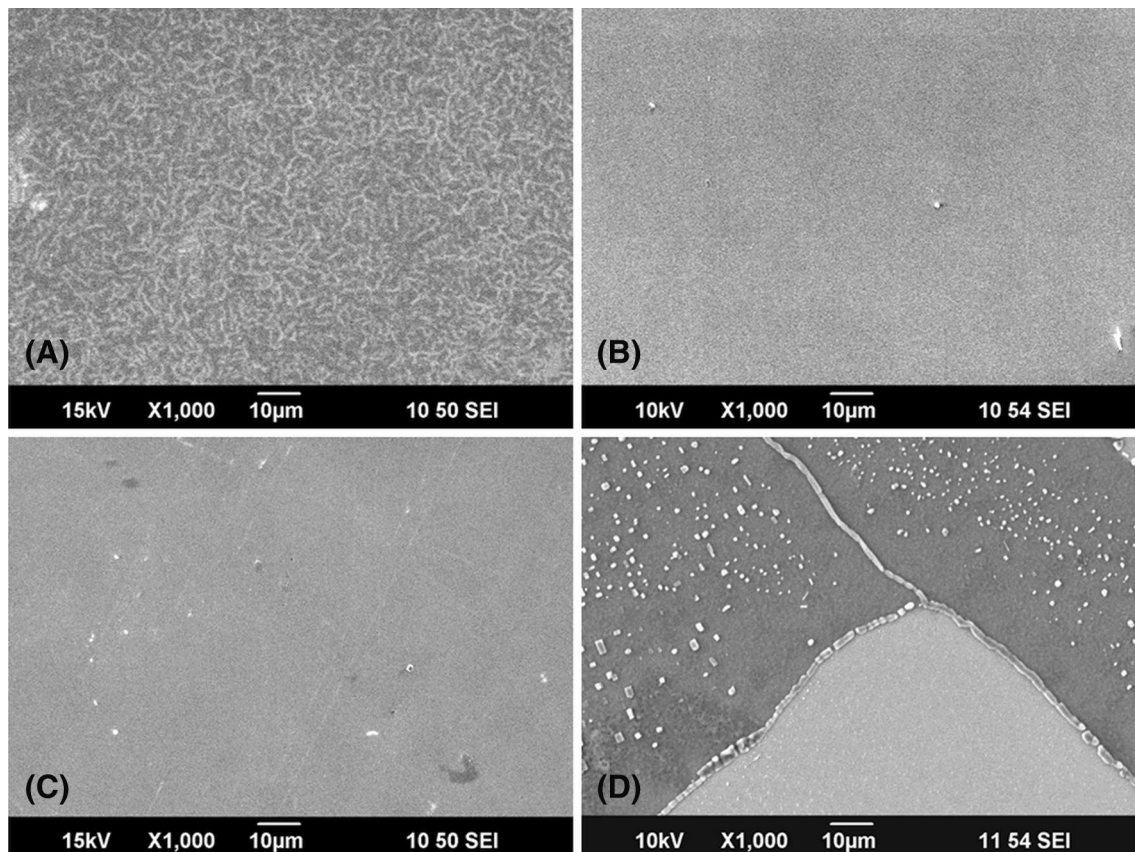
Fig. 7 SEM micrographs (×1000 magnification) of the disks surfaces after tests with: **a** RPMI, **b** RPMI + BSA, **c** RPMI + HA, **d** RPMI + HA + BSA—both the surface and the film are visible in this spot

Table 4 Representative results of EDS measurements which allowed for identification of the nature of the deposits observed after the electrochemical tests

Electrolyte	Spot/area	Elements (wt%)									
		O	C	Si	Mo	Cr	Co	P	S	Na	Cl
RPMI	Film	8.90	7.42	0.67	5.15	25.1	52.8	–	–	–	–
RPMI+BSA	Film	8.97	11.4	–	5.36	26.8	47.4	–	–	–	–
RPMI+HA	Film	6.76	5.5	–	6.61	26.7	54.5	–	–	–	–
RPMI+HA+BSA	Film	9.21	4.99	–	6.33	20.6	43.0	1.61	–	–	–
	Coating	38.8	52.8	–	–	1.78	–	–	1.48	2.38	2.73
Discs' surface		–	–	–	4.12	31.1	64.6	–	–	–	–
CoCrMo-LC		–	0.03	0.38	5.7	27.6	65.5	–	–	–	–
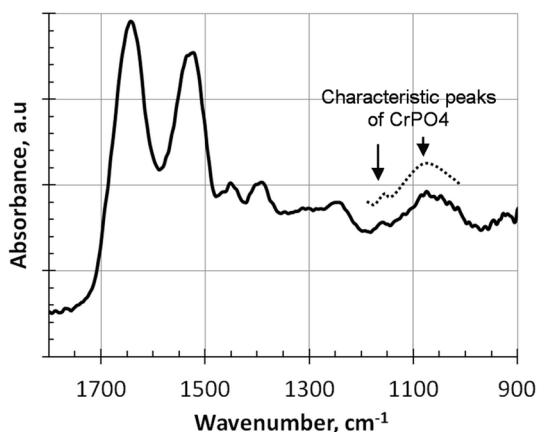
Fig. 8 FTIR spectrum of the film on specimen tested in RPMI+HA+BSA. The dashed line between 1200 and 1000 cm^{-1} gives a qualitative indication of a characteristic spectrum of CrPO$_4$

The films on specimens tested in RPMI, RPMI+BSA and RPMI+HA consisted of organic material and were too thin to be analyzed separately from the passive oxide film. The films on the specimens tested in RPMI+HA+BSA contained organic material and the presence of mineral elements (P, Na, Cl). Flakes from the green coating analyzed separately were organic and contained Cr, S, Na, and Cl.

FTIR spectroscopy was used to analyze the film resulting from the RPMI+HA+BSA electrolyte (Fig. 8). Protein associated Amide I/II peaks were observed at 1640 cm^{-1} and 1520 cm^{-1}, respectively. Compared to naïve BSA spectrum, both peaks presented red-shifted suggesting changes in conformational structure of BSA residual after experiments. Peaks between 1200 and 1000 cm^{-1} were measured possibly corresponding to the $\nu1$ and $\nu3$ peaks of CrPO$_4$ indicating the formation of phosphate in the film. The similar spectrum of collagen/phosphate mixture from a retrieval study was reported in the previous literature [40].

4 Discussion

4.1 Model Synovial Fluid

Cell culture medium is proposed here as a more complex and richer solvent for model synovial fluids compared to phosphate-buffered saline (PBS) solution or simulated body fluid (SBF). For comparison, the molar concentrations of the inorganic salts in RPMI-1640, PBSA and SBF are displayed in Table 5 (SBF from [33]; PBS from [37]). Corresponding ionic concentrations can be found in a recent publication about the suitability of cell culture medium for the biocompatibility assessment of metallic biomaterials [31]. In addition to inorganic salts, RPMI-1640 also contains amino acids and vitamins for nutrition of cells. Similarly, natural synovial fluid guarantees the nutrition for chondrocytes and cartilage. In this regard, a previous study pointed out the relevance of the minerals present in synovial fluid [41]. The reported mean concentrations of mineral elements in synovial fluid of healthy bovine joints were (in mM): 0.78 for Ca, 0.37 for Mg, 1.47-2.16 for P, 3.90 for K, 124 for Na and 107 for Cl. Considering their presence in the base test fluids of Table 5, the cell culture medium RPMI-1640 has comparable concentrations of Mg, K and Na, 2 times less Ca, 2-3 times more P and about 10 times less Cl. In addition, the choice of the cell culture medium RPMI-1640 as solvent electrolyte was triggered by the aim to ultimately run tribocorrosion tests in the presence of cells. A similar approach

Table 5 Concentration inorganic salts (mM) of RPMI-1640 compared to typical base fluids used in tribocorrosion studies (*SBF* simulated body fluid, *PBS* phosphate buffered solution; see text for references)

Base fluid	Inorganic salts contents (mM)									
	NaCl	KCl	MgSO$_4$	KH$_2$PO$_4$	CaCl$_2$	MgCl$_2$	NaHCO$_3$	Na$_2$SO$_4$	Ca(NO$_3$)$_2$	Na$_2$HPO$_4$
RPMI	103.4	5.3	0.41	–	–	–	23.8	–	0.42	5.63
SBF	140	3	–	1	2.5	1500	4.2	0.5	–	–
PBS	140	3	–	1	–	–	–	–	–	10

has been previously reported by the group of Merritt and Brown early in the 90s [42–45]. In [45], RPMI-1640 was used with additions of $CaCl_2$ and H_2O_2 in fretting and corrosion tests with Ti6Al4V. Impergre et al. [31] have accurately evaluated the intrinsic electrochemical reactivity of RPMI by comparing the three following different electrolytes in a Platinum–Platinum-SCE 3-electrode-cell configuration: RPMI-1640 supplemented with 10% fetal bovine serum and 1% antibiotic–antimycotic; Dulbecco's phosphate-buffered saline solution; and a self-made RPMI-1640 solution. They found that the reactivity of the organic compounds of supplemented RPMI-1640 takes place in the same potential field of the passive domain of cobalt alloy. Additionally, the influence of the atmosphere (aerated, non-aerated or with 5% CO_2 inside the incubator) was also investigated, and the addition of 5% CO_2 in air content was found to decrease the rate of redox reactions. Their conclusions strongly support the use of cell culture medium for studying the passivation behavior of biomaterials. Finally, when discussing the choice of cell culture medium as alternative solvent to PBS solution or SBF for model synovial fluids, characteristic electrochemical values like the OCP can be used as criteria for comparison: according to our results and to results published in literature, the OCP of CoCrMo in RPMI lies in-between OCP values measured in PBS [28, 46] and human synovial fluids [46].

4.2 Electrochemical Measurements

The results corresponding to four different electrolytes groups (RPMI, RPMI + BSA, RPMI + HA, RPMI + HA + BSA) in a 5-step sequence of electrochemical measurements were presented above. The decrease in the initial OCP values observed with addition of BSA to the base fluid is in agreement with the literature [28–30], as well as the increase in OCP values in the presence of HA [25]. The plots from the polarization measurements exhibited a similar behavior for all electrolytes in both cathodic and anodic domains, with differences mainly in characteristic potential and current values. During *cathodic polarization*, all electrolytes showed a considerable negative shift of the cathodic E_{CORR}. This shift was more accentuated with BSA containing electrolytes, conforming the cathodic inhibitor role of BSA as described in the literature [28–30]. During anodic polarization, the presence of HA led to higher current values at the end of the forward scan, with steeper decreases at the beginning of the reverse scan; this was related to the formation of organic films. Recently, we have investigated the role played by HA on the corrosion resistance of CoCrMo, in conditions of active dissolution of the passive film triggered by addition of hydrogen peroxide reagent into solution [36]. We have found out that, in a saline serum solution containing 30 mM H_2O_2, the corrosion resistance of CoCrMo is significantly lower with HA, than without HA; to explain this finding, we have considered the mechanism of preferential complexation of the HA macromolecules with the metal ions released from the alloy, which has been speculated in literature [35, 47, 48]. The experimental results of the present manuscript support such a mechanism, whereby the release of metals ions from the alloy is triggered here by anodic polarization, instead of by the oxidizing effect of H_2O_2 [36] or tribocorrosion [47]. Interestingly, the results from the EIS equivalent circuit analysis at open circuit potential revealed the corrosive action of HA alone, without proteins in solution; this suggests, that adsorbed proteins did not withstand the step of forward anodic polarization.

4.3 Surface Analysis

The isoelectric point of the CoCrMo-alloy surface is given by the Cr_2O_3 oxide film, and it is in the range of 6.2–8.1 [49]. The pH of the cell culture medium was generally kept stable at 7.4 thanks to the carbonate-based buffer in the 5% CO_2 atmosphere. This means, that the CoCrMo-alloy surface had generally a neutral charge, and protein absorption was governed by hydrophobic interaction [26]; according to [50], hydrophobic surfaces favor irreversible adsorption of proteins, and irreversibly adsorbed proteins cannot be displaced by an incoming large proteins; therefore, also the HA macromolecules were not able to displace the adsorbed proteins. Gispert et al. [20] investigated wettability of different biomaterials in model synovial fluids containing HA and BSA, confirming a high stability of the adsorbed albumin layer formed on CoCrMo-surface, even in the presence of HA. In our study, anodic polarization in the presence of HA caused a decrease in local pH of the CoCrMo-metal surface, as indicated by the yellow coloration of the cell culture medium. The isoelectric point of HA is 2.5 [51], and the isoelectric point of BSA is 4.7–4.9 [26]: during the step of reverse anodic polarization, precipitation of HA-BSA complexes occurred [52] on the top of the adsorbed proteins layer. The CoCrMo disks were analyzed using SEM/EDS after the electrochemical experiments. All samples were covered by an organic film. This finding is generally recognized in the literature when protein-containing media are used. In particular, the appearance of a carbonaceous film has been related to the presence of Mo in the CoCrMo alloy [53]. Samples tested in the electrolyte group "RPMI + HA + BSA" showed two main differences with regard to samples tested in the other electrolyte groups: the presence of phosphorus in the organic film and the precipitation of an organic gel containing the elements Cr, S, Na and Cl. This finding has potentially clinical relevance, because chromium phosphates and sulfate-containing debris have been reported from pathological tissues retrieved after total hip replacement [54, 55]. Some studies have pointed out

the role of phosphate ions in electrochemical experiments: in [25], the formation of calcium phosphate on CoCrMo alloy was found to be stimulated by HA dissolved in NaCl solutions and Hank's solutions; the influence of phosphate ions on the corrosion behavior of CoCrMo in protein containing simulated body fluids has been demonstrated [27, 28]. No literature has been found on the possible generation of chromium phosphate $CrPO_4$ as corrosion product after anodic treatments of CoCrMo alloy in model synovial fluids. Based on our FTIR results, the presence of $CrPO_4$ in the films generated by RPMI + HA + BSA solutions is highly likely. Further investigations are necessary to identify anodization products generated on CoCrMo alloy in laboratory tests with respect to their clinical relevance.

4.4 Limitations and Outlook

This study has several limitations. First, the electrochemical reactions involved during the cathodic and anodic polarization could not be tracked due to the complexity of the solvent medium (RPMI-1640); these reactions masked the CoCrMo passivation plateau typically seen in other electrolytes such as Ringer's solution, buffer solution and bovine calf serum [53] as well as in human synovial fluid [46]. Second, the model synovial fluid used in this study does not contain other types of proteins and other components which—even if present in smaller concentrations than the albumin proteins and hyaluronic acid—may also contribute to the electrochemical behavior of CoCrMo alloy. Finally, there is no evidence for the clinical occurrence of potential variations within the range tested by this study. The test samples were polarized to potential values exceeding transpassive dissolution, which are unlikely to occur under actual physiological conditions.

5 Conclusions

The results of this study confirmed the cathodic inhibitor role of albumin proteins (BSA) already established in the literature, and indicated the following new findings about hyaluronic acid (HA): the presence of hyaluronic acid altered the reactions involved in the protective passive film growth and its dissolution in the transpassive potential domain, resulting in lower corrosion resistance, and higher anodic currents. In addition, hyaluronic acid molecules interacted with BSA proteins forming complexes which precipitate during anodization, presumably due to a local pH decrease. Finally, only in the presence of both HA and BSA a phosphorus containing film resulted, suggestive of the phosphate corrosion products found in vivo. Based on these results, it can be stated that it is important, for more clinically relevant

results, to add hyaluronic acid to lubricants in tribocorrosion tests with CoCrMo alloys.

Compliance with Ethical Standards

Conflict of interest The authors have no conflicts of interest to declare.

References

1. De Martino I, Assini JB, Elpers ME, Wright TM, Westrich GH (2015) Corrosion and fretting of a modular hip system: a retrieval analysis of 60 rejuvenate stems. J Arthroplast 30(8):1470–1475. https://doi.org/10.1016/j.arth.2015.03.010
2. Shahgaldi BF, Heatley FW, Dewar A, Corrin B (1995) In vivo corrosion of cobalt-chromium and titanium wear particles. J Bone Joint Surg Br 77(6):962–966
3. Mischler S, Igual Munoz A (2013) Wear of CoCrMo alloys used in metal-on-metal hip joints: a tribocorrosion appraisal. Wear 297:1081–1094
4. Milošev I, Remškar M (2009) In vivo production of nanosized metal wear debris formed by tribochemical reaction as confirmed by high-resolution TEM and XPS analyses. J Biomed Mater Res Part A 91A(4):1100–1110. https://doi.org/10.1002/jbm.a.32301
5. Matusiewicz H (2014) Potential release of in vivo trace metals from metallic medical implants in the human body: from ions to nanoparticles: a systematic analytical review. Acta Biomater 10(6):2379–2403
6. Hart AJ, Quinn PD, Sampson B, Sandison A, Atkinson KD, Skinner JA, Powell JJ, Mosselmans JFW (2010) The chemical form of metallic debris in tissues surrounding metal-on-metal hips with unexplained failure. Acta Biomater 6(11):4439–4446. https://doi.org/10.1016/j.actbio.2010.06.006
7. Cadosch D, Chan E, Gautschi OP, Filgueira L (2009) Metal is not inert: role of metal ions released by biocorrosion in aseptic loosening–current concepts. J Biomed Mater Res A 91(4):1252–1262
8. Afolaranmi GA, Tettey J, Meek RM, Grant MH (2008) Release of chromium from orthopaedic arthroplasties. Open Orthop J 2:10–18
9. Liu HC, Guo F, Wong PL, Li X (2017) Investigation of adsorbed protein and passive films on hydrodynamic lubricated steel slider surface. Tribol Int 109:133–139. https://doi.org/10.1016/j.triboint.2016.12.034
10. Wu BJ, Deng QY, Leng YX, Wang CM, Huang N (2016) or 2017) Characterization of adsorption and lubrication of synovial fluid proteins and HA on DLC joint bearings surface. Surf Coat Technol. https://doi.org/10.1016/j.surfcoat.2016.12.058
11. Yan Y, Neville A, Dowson D (2007) Biotribocorrosion of CoCrMo orthopaedic implant materials—assessing the formation

and effect of the biofilm. Tribol Int 40(10–12):1492–1499. https ://doi.org/10.1016/j.triboint.2007.02.019

12. Catelas I, Wimmer MA (2011) New insights into wear and biological effects of metal-on-metal bearings. J Bone Joint Surg Am 93(2):76–83. https://doi.org/10.2106/jbjs.j.01877

13. Mathew MT, Nagelli C, Pourzal R, Fischer A, Laurent MP, Jacobs JJ, Wimmer MA (2014) Tribolayer formation in a metal-on-metal (MoM) hip joint: an electrochemical investigation. J Mech Behav Biomed Mater 29:199–212. https://doi.org/10.1016/j.jmbbm.2013.08.018

14. Wimmer MA, Mathew MT, Laurent MP, Nagelli C, Liao Y, Marks LD, Pourzal R, Fischer A, Jacobs JJ (2013) Tribochemical reactions in metal-on-metal hip joints influence wear and corrosion. ASTM Special Technical Publication 1560 STP: 1–18. doi:https://doi.org/10.1520/stp156020120050

15. Serro AP, Gispert MP, Martins MC, Brogueira P, Colaco R, Saramago B (2006) Adsorption of albumin on prosthetic materials: implication for tribological behavior. J Biomed Mater Res A 78(3):581–589

16. Alves CFA, Oliveira F, Carvalho I, Piedade AP, Carvalho S (2014) Influence of albumin on the tribological behavior of Ag–Ti (C, N) thin films for orthopedic implants. Mater Sci Eng C 34:22–28. https://doi.org/10.1016/j.msec.2013.09.031

17. Catelas I, Bobyn JD, Medley JB, Krygier JJ, Zukor DJ, Huk OL (2003) Size, shape, and composition of wear particles from metal–metal hip simulator testing: effects of alloy and number of loading cycles. J Biomed Mater Res Part A 67A(1):312–327. https://doi.org/10.1002/jbm.a.10088

18. Mathew MT, Uth T, Hallab NJ, Pourzal R, Fischer A, Wimmer MA (2011) Construction of a tribocorrosion test apparatus for the hip joint: validation, test methodology and analysis. Wear 271(9–10):2651–2659. https://doi.org/10.1016/j.wear.2011.01.085

19. Bortel E, Charbonnier B, Heuberger R (2015) Development of a synthetic synovial fluid for tribological testing. Lubricants 3(4):664

20. Gispert M, Serro A, Colaco R, Saramago B (2006) Friction and wear mechanisms in hip prosthesis: comparison of joint materials behaviour in several lubricants. Wear 260(1):149–158

21. Mathew MT, Srinivasa Pai P, Pourzal R, Fischer A, Wimmer MA (2009) Significance of tribocorrosion in biomedical applications: overview and current status. Adv Tribol 2009:12. https://doi.org/10.1155/2009/250986

22. Galandakova A, Ulrichova J, Langova K, Hanakova A, Vrbka M, Hartl M, Gallo J (2017) Characteristics of synovial fluid required for optimization of lubrication fluid for biotribological experiments. J Biomed Mater Res B 105(6):1422–1431

23. Takadama H, Mizuno M (2006) A simulated synovial fluid for wear characterization of artificial hip joints by a hip joint simulator. Key Eng Mater 309–311:1273–1276

24. Karimi S, Alfantazi AM (2014) Ion release and surface oxide composition of AISI 316L, Co-28Cr-6Mo, and Ti-6Al-4V alloys immersed in human serum albumin solutions. Mater Sci Eng C 40:435–444

25. Milošev I, Hmeljak J, Cör A (2013) Hyaluronic acid stimulates the formation of calcium phosphate on CoCrMo alloy in simulated physiological solution. J Mater Sci 24(3):555–571. https://doi.org/10.1007/s10856-012-4827-8

26. Yan Y, Yang H, Su Y, Qiao L (2015) Albumin adsorption on CoCrMo alloy surfaces. Sci Rep 5:18403. https://doi.org/10.1038/srep18403

27. Ouerd A, Alemany-Dumont C, Normand B, Szunerits S (2008) Reactivity of CoCrMo alloy in physiological medium: electrochemical characterization of the metal/protein interface. Electrochim Acta 53(13):4461–4469. https://doi.org/10.1016/j.electacta.2008.01.025

28. Muñoz AI, Mischler S (2007) Interactive effects of albumin and phosphate ions on the corrosion of CoCrMo implant alloy. J Electrochem Soc 154(10):C562–C570

29. Valero Vidal C, Olmo Juan A, Igual Munoz A (2010) Adsorption of bovine serum albumin on CoCrMo surface: effect of temperature and protein concentration. Colloids Surf B 80(1):1–11

30. Munoz AI, Mischler S (2015) Electrochemical quartz crystal microbalance and X-Ray photoelectron spectroscopy study of cathodic reactions in bovine serum albumin containing solutions on a physical vapour deposition-CoCrMo biomedical alloy. Electrochim Acta 180:96–103. https://doi.org/10.1016/j.electacta.2015.08.017

31. Impergre A, Ter-Ovanessian B, Der Loughian C, Normand B (2018) Systemic strategy for biocompatibility assessments of metallic biomaterials: representativeness of cell culture medium. Electrochim Acta 283:1017–1027. https://doi.org/10.1016/j.electacta.2018.06.196

32. Bard AJ, Faulkner LR (2000) Electrochemical methods: fundamentals and applications. Wiley, Austin

33. Hodgson AWE, Kurz S, Virtanen S, Fervel V, Olsson COA, Mischler S (2004) Passive and transpassive behaviour of CoCrMo in simulated biological solutions. Electrochim Acta 49(13):2167–2178. https://doi.org/10.1016/j.electacta.2003.12.043

34. Ponthiaux P, Wenger F, Celis J-P (2012) Tribocorrosion: material behavior under combined conditions of corrosion and mechanical loading. In: Shih H (ed) Corrosion resistance. IntechOpen. https://doi.org/10.5772/35634

35. Khobragade N, Bansod AV, Giradkar KV, Patil A, Jagtap K, Pawde R, Moon A (2018) Effect of concentration and surface roughness on corrosion behavior of Co–Cr–Mo Alloy in hyaluronic acid. Mater Res Exp. https://doi.org/10.1088/2053-1591/aaa5f2

36. Radice S, Yao J, Babauta J, Laurent MP, Wimmer MA (2019) The effect of hyaluronic acid on the corrosion of an orthopedic CoCrMo-alloy in simulated inflammatory conditions. Materialia 6:100348. https://doi.org/10.1016/j.mtla.2019.100348

37. Valero-Vidal C, Igual Muñoz A, Olsson C-OA, Mischler S (2012) Passivation of a CoCrMo PVD alloy with biomedical composition under simulated physiological conditions studied by EQCM and XPS. J Electrochem Soc 159(5):C233–C243. https://doi.org/10.1149/2.090205jes

38. Cann PM, Spikes HA, Hutchinson J (1996) The development of a spacer layer imaging method (SLIM) for mapping elastohydrodynamic contacts. Tribol Trans 39(4):915–921. https://doi.org/10.1080/10402009608983612

39. Fischer A, Janssen D, Wimmer MA (2017) The influence of molybdenum on the fretting corrosion behavior of CoCr/TiAlV couples. Biotribology. https://doi.org/10.1016/j.biotri.2017.01.001

40. Liu S, Hall DJ, McCarthy SM, Jacobs JJ, Urban RM, Pourzal R (2019) Fourier transform infrared spectroscopic imaging of wear and corrosion products within joint capsule tissue from total hip replacements patients. J Biomed Mater Res B. https://doi.org/10.1002/jbm.b.34408

41. Scholz H, Karatzias H, Stoeber M (1983) Mineralstoffkonzentrationen in der Synovia des gelenksgesunden Rindes. Zbl Vet Med A 30:348–354

42. Merritt K, Wenz L, Brown SA (1991) Cell association of fretting corrosion products generated in a cell culture. J Orthop Res 9(2):289–296. https://doi.org/10.1002/jor.1100090218

43. Merritt K, Brown SA (1995) Release of hexavalent chromium from corrosion of stainless steel and cobalt-chromium alloys. J Biomed Mater Res 29(5):627–633

44. Merritt K, Brown SA (1996) Distribution of cobalt chromium wear and corrosion products and biologic reactions. Clin Orthop Relat Res 329(43):S233–S243

45. Montague A, Merritt K, Brown S, Payer J (1996) Effects of Ca and H_2O_2 added to RPMI on the fretting corrosion of Ti6Al4V. J Biomed Mater Res 32(4):519–526

46. Munoz A, Schwiesau J, Jolles BM, Mischler S (2015) In vivo electrochemical corrosion study of a CoCrMo biomedical alloy in human synovial fluids. Acta Biomater 21:228–236. https://doi.org/10.1016/j.actbio.2015.03.008

47. DesJardins J, Aurora A, Tanner SL, Pace TB, Acampora KB, Laberge M (2006) Increased total knee arthroplasty ultra-high molecular weight polyethylene wear using a clinically relevant hyaluronic acid simulator lubricant. Proc Inst Mech Eng H 220(5):609–623. https://doi.org/10.1243/09544119JEIM30

48. Garcia-Alonso MC, Llorente I, Diaz I, Escudero ML (2018) Interaction of hyaluronic acid with CoCr alloy under immersion and wear–corrosion processes. Tribol Lett 66(4):122. https://doi.org/10.1007/s11249-018-1073-3

49. Scientific H (2011) Determination of the isoelectric point using zeta potential. Saved from URL: https://www.azomcom/articleaspx?ArticleID=5829

50. Pandey LM, Pattanayek SK (2013) Properties of competitively adsorbed BSA and fibrinogen from their mixture on mixed and hybrid surfaces. Appl Surf Sci 264:832–837. https://doi.org/10.1016/j.apsusc.2012.10.150

51. Gatej I, Popa M, Rinaudo M (2005) Role of the pH on hyaluronan behavior in aqueous solution. Biomacromol 6(1):61–67. https://doi.org/10.1021/bm040050m

52. Xu S, Yamanaka J, Sato S, Miyama I, Yonese M (2000) Characteristics of complexes composed of sodium hyaluronate and bovine serum albumin. Chem Pharm Bull 48(6):779–783

53. Martin EJ, Pourzal R, Mathew MT, Shull KR (2013) Dominant role of molybdenum in the electrochemical deposition of biological macromolecules on metallic surfaces. Langmuir 29(15):4813–4822. https://doi.org/10.1021/la304046q

54. Urban RM, Jacobs JJ, Gilbert JL, Galante JO (1994) Migration of corrosion products from modular hip prostheses. Particle microanalysis and histopathological findings. J Bone Joint Surg Am 76(9):1345–1359

55. Jacobs JJ, Gilbert JL, Urban RM (1998) Current concepts review-corrosion of metal orthopaedic implants. J Bone Joint Surg Am 80(2):268–282